NASA MEMO 12-29-58E

NASA

MEMORANDUM

PROPELLANT VAPORIZATION AS A CRITERION FOR ROCKET-ENGINE DESIGN; EXPERIMENTAL PERFORMANCE, VAPORIZATION, AND HEAT-TRANSFER RATES WITH VARIOUS PROPELLANT COMBINATIONS

By Bruce J. Clark, Martin Hersch, and Richard J. Priem

Lewis Research Center
Cleveland, Ohio

NATIONAL AERONAUTICS AND SPACE ADMINISTRATION
WASHINGTON
January 1959

NATIONAL AERONAUTICS AND SPACE ADMINISTRATION

MEMORANDUM 12-29-58E

PROPELLANT VAPORIZATION AS A CRITERION FOR ROCKET-ENGINE DESIGN; EXPERIMENTAL PERFORMANCE, VAPORIZATION, AND HEAT-TRANSFER RATES WITH VARIOUS PROPELLANT COMBINATIONS

By Bruce J. Clark, Martin Hersch, and Richard J. Priem

SUMMARY

Experimental combustion efficiencies of eleven propellant combinations were determined as a function of chamber length. Efficiencies were measured in terms of characteristic exhaust velocities at three chamber lengths and in terms of gas velocities. The data were obtained in a nominal 200-pound-thrust rocket engine. Injector and engine configurations were kept essentially the same to allow comparison of the performance.

The data, except for those on hydrazine and ammonia-fluorine, agreed with predicted results based on the assumption that vaporization of the propellants determines the rate of combustion. Decomposition in the liquid phase may be responsible for the anomalous behavior of hydrazine.

Over-all heat-transfer rates were also measured for each combination. These rates were close to the values predicted by standard heat-transfer calculations except for the combinations using ammonia.

INTRODUCTION

The importance of the vaporization process in rocket-engine combustion was indicated in a previous experimental study (ref. 1) of the effect of injection processes on engine performance. This study showed qualitatively that atomization of the slower vaporizing propellant gave the greatest increase in combustion efficiency. Recent analytical studies (refs. 2 to 5), based on the concept of propellant vaporization as the rate-controlling combustion process, have shown how changes in drop size, gas velocity, drop velocities, chamber pressure, propellant temperature, and propellant type affect combustor performance. Qualitatively, these calculations agree with the available data. However, specific studies of each of these variables under controlled test conditions are required to evaluate the concept. The vaporization-rate calculations for heptane, ammonia, hydrazine, oxygen, and fluorine (ref. 5) indicated that there would be large differences in combustion efficiency with these propellants. The purpose of this report is to show the effect of these propellants on experimental combustion efficiency and heat-transfer rate, and to relate these results to the analytical vaporization rates of reference 5 and to calculated heat-transfer rates.

Eleven different propellant combinations were tested under controlled conditions in one type and thrust-level engine. One propellant was injected either as a finely atomized spray or as a gas, and the second propellant was injected as a relatively coarse spray from a pair of impinging jets so that the vaporization rate of the second propellant would be slower than that of the first. The injection velocity and orifice diameter for the second propellant were kept constant for all the combinations in order to limit the variations in drop size to effects due to differences in propellant properties. By this method, it was possible to determine the effect on performance of changing the propellant and to compare apparent vaporization rates.

The experimental data are presented in graphical form to show the effect of propellant changes on combustion efficiency. The comparison with analytical results is presented in terms of the percent of one propellant unvaporized.

APPARATUS AND PROCEDURE

Rocket Engine

Tests were run in a rocket engine designed for a nominal 200-pound thrust with heptane-oxygen at a 300-pound-per-square-inch chamber pressure (fig. 1). The injector, combustion chamber, and nozzle were separable units. The engine had a contraction ratio of 6.4 and a throat diameter of 0.79 inch. Solid uncooled chambers 1 and 3 inches long and a water-cooled chamber 8 inches long were used.

Injectors for liquid-liquid and liquid-gaseous propellant combinations were similar (figs. 2 and 3). One liquid propellant was sprayed into the chamber in a flat sheet from two impinging jets of 0.089-inch diameter. When the second propellant was liquid, it was introduced through two parallel rows of 0.032-inch holes to form sprays parallel to the spray sheet of the other propellant. Gaseous propellants were introduced behind the spray of the impinging jets through a diffuser with a 15° half-angle. With liquid-liquid propellant combinations, the fuel was always the propellant in the impinging jets. With gaseous-liquid combinations, the liquid was atomized by the impinging jets.

Performance Measurements

Chamber pressure was measured both by a recording Bourdon-tube-type instrument and by a strain-gage transducer with output recorded on a galvanometer-type instrument.

Liquid fuel and liquid oxidant flow rates and coolant water rate were measured by rotating-vane meters. A sharp-edged orifice was used to measure gaseous flow rates. The pressure and temperature of the gas upstream of the orifice were measured with a Bourdon-tube instrument and an iron-constantan thermocouple. Orifice pressure drop was measured by strain gages read on potentiometer- and galvanometer-type recording instruments. Iron-constantan thermocouples were used to measure propellant temperatures and coolant water temperatures. Gas velocities were measured by streak photography through a transparent plastic chamber by the method of reference 1.

Pressure transducers had a maximum error of ±1 percent and the maximum error of the flowmeters was ±2 percent, so that the maximum possible error in c^* values was ±3 percent. A complete list of symbols used in this report is given in appendix A. Actual reproducibility of c^* was approximately ±2 percent; five or more runs were used to determine average c^* values. Errors in temperature measurements allowed a heat-transfer error of ±10 percent. Maximum error of gas velocities measured by streak photography was estimated as ±20 percent.

Experimental Procedure

Table I lists the various propellant combinations that were investigated, including the maximum theoretical c^* values and corresponding mixture ratios. The effects of the mixture ratios on theoretical c^* values (refs. 6 to 10 and unpublished NASA data) are shown in figure 4. In table I the oxidant and fuel weight flows and injection velocities are given for these mixture ratios with a constant velocity in the impinging jets. The resultant chamber pressures at 100 percent efficiency and the propellant temperatures measured during the tests are also listed.

Only runs with weight flows within ±5 percent of the values in table I were used for data. Chamber pressure and weight flows were measured to determine experimental c^* values. Test firings were of approximately 3 seconds duration.

RESULTS AND DISCUSSION

Performance Comparisons

The experimental engine data for each run are listed in table II. Average experimental data are presented in figure 5 as the variation of combustion efficiency η_c with chamber length for each propellant combination.

For the liquid fuels (heptane, ammonia, and hydrazine) the η_c (fig. 5(a)) with liquid oxygen was approximately the same as with gaseous oxygen. With liquid fluorine, ammonia and hydrazine gave lower efficiencies than with either liquid oxygen or gaseous oxygen. Liquid oxygen and liquid fluorine gave approximately the same efficiency with hydrogen.

Of all the fuels used, gaseous hydrogen with any oxidant generally burned with the highest efficiency (fig. 5(b)). In the 8-inch chamber length the combustion efficiency of the liquid oxygen - gaseous methane combination was greater than the efficiencies of the liquid oxygen - liquid fuel combinations but less than the liquid oxygen - gaseous hydrogen combination.

Within the limits of experimental accuracy the η_c of heptane, ammonia, and hydrazine with liquid and gaseous oxygen were the same in an 8-inch chamber. When burned with fluorine, ammonia gave a lower performance than hydrazine. In the shorter chamber lengths, hydrazine gave higher performance values with oxygen than the other fuels (except hydrogen).

Figure 6 shows a comparison of combustion efficiencies based on c^* measurements with efficiencies from gas velocity measurements. Gas velocities were converted to efficiencies by dividing by the gas velocity that would occur in the chamber at theoretical c^*, as in reference 1. For the 8-inch chamber lengths efficiencies as determined from measured gas velocities agree well with efficiencies determined from c^* values. As was found in reference 11, efficiencies from c^* values in the shorter chamber lengths are higher than efficiencies from gas velocities for corresponding points within an 8-inch chamber; the reason for this is suggested in a later section of this report.

Vaporization-Rate Comparisons

Reference 5 presents an analytical correlation between percent vaporized and an effective length for various propellants, where:

$$\text{Effective length} = \frac{L\ P^{0.66} u_{fin}^{0.4} (1.9\times10^{-5})}{(1 - T^{*})^{0.4} V_0^{0.75} M_{g,m}^{1.45}} \tag{1}$$

To compare these experimental results with the analytical data of reference 5, the combustion efficiencies were converted to a percent of one propellant vaporized (ref. 4); this assumes that the vaporization of this propellant controls the combustion rate. Experimental gas velocity data were corrected to percent of one propellant vaporized by the technique described in appendix B. The actual chamber length was converted to an effective length by using the appropriate conversion factors as described hereafter.

The initial propellant temperature and the chamber pressure were measured directly. Injection velocity was obtained from the measured flow rate and the injector orifice area. The final gas velocity was calculated from isentropic flow relations and actual engine efficiency as shown in appendix C. For the total chamber length L, $1\frac{3}{4}$ inches were added to the cylindrical length of the chamber to account for the effect of the gases accelerating to the nozzle throat.

The mass median drop size was determined by combining the following correlations obtained in references 12 and 13. For impinging jets of heptane,

$$\frac{D_j}{D_{30}} = 2.64\sqrt{D_j V_j} + 0.97\ D_j\ \Delta V \tag{2}$$

For crosscurrent breakup of jets of various liquids,

$$D_{30} \propto \left(\frac{\sigma\mu_l}{\rho_l \rho_s}\right)^{1/4} \tag{3}$$

The mass median drop size $M_{g,m}$ can be related to the volume mean drop size D_{30} for any particular drop-size distribution. For the distribution found in reference 12, $M_{g,m}$ is within a few percent of $0.75\ D_{30}$.

In equation (2) the jet diameter and jet velocity were determined from experimental conditions. However, the gas velocity surrounding the jet cannot be determined in this manner. In reference 12 the stream of air had a constant velocity; in a rocket engine, as the propellants vaporize, this velocity increases from zero at the injector face to the velocity at the nozzle inlet. An average value of 100 feet per second was assumed for these calculations. This velocity may represent that obtained in the first quarter of the chamber, or it may represent velocity perturbations produced by small pressure fluctuations. The propellant properties in equation (3) were evaluated at the injection temperatures shown in table I. It is assumed herein that the effect of liquid properties on the drop sizes formed by impinging jets will be the same as for crosscurrent jets.

Comparison of Experimental and Analytical Data

Figure 7 shows the percent mass unvaporized of the controlling propellant determined from experimental data, as a function of the effective length calculated by equation (1). For each vaporizing propellant the correlation of the data obtained with different combinations is good. In the cases of heptane, liquid oxygen, and fluorine the spread of the experimental data is less than the spread in the analytical results of reference 5, as shown by the shaded area. For ammonia and hydrazine the experimental spread is larger than the analytical spread.

The experimental data agree fairly well with the analytically predicted values except for ammonia-fluorine and the combinations involving hydrazine. The experimental points indicate that ammonia-fluorine burns more slowly than is predicted by vaporization-rate calculations and that hydrazine burns faster than predicted. A possible explanation for the discrepancies with hydrazine may be the fact that hydrazine decomposes at about 1000° R (ref. 14), which is about the temperature the drop reaches as it vaporizes. This decomposition, if sufficiently rapid, could cause the drops to shatter and thus result in a higher vaporization rate. A slow decomposition rate would add heat to the drops without shattering them. This additional heat, which was not considered in the analytical calculations, would also result in a higher vaporization rate. Another possible explanation for the deviation in the results for hydrazine may be the unusually large drop size calculated for hydrazine by equation (3), due to the high surface tension of hydrazine. This large drop size decreased the effective length by 45 percent. Thus, the data for hydrazine may be overcorrected for drop size.

The curves shown in figure 6 indicated that the combustion efficiency as determined from c^* measurement in a short engine is higher than that determined from gas velocity measurement at the same intermediate point in a long engine. This can be predicted by the analytical model of vaporization-limited combustion. The gas velocity at a point in the short engine is much higher than at that point in the long engine because of the lower pressure and density at lower efficiency (this effect of density on gas velocity is explained in appendix C). The higher gas velocity would result in an increased vaporization rate, giving higher combustion efficiency in the short engine. The measured gas velocity data agree with measured $c*$ data when compared on the basis of vaporization rates, as shown in figure 7.

Heat-Transfer Comparison

Experimental heat-transfer rates for the various propellant combinations in a water-cooled 8-inch chamber are listed in table III. Calculated heat-transfer rates for the same combinations at 100 percent combustion efficiency are also listed. In order to compare the analytical and experimental rates, analytical rates for 100 percent combustion efficiency were modified for the actual efficiency and gas velocity distribution of the engine, as described in appendix D.

Table III shows that the experimental heat-transfer rates were between 5 percent higher and 21.6 percent lower than these corrected analytical rates, except for the propellant combinations involving liquid ammonia.

The low heat-transfer rates with ammonia may be due to film cooling with the ammonia. Gas-side wall temperatures calculated from the experimental heat-transfer rates, and the boiling points of the controlling propellants at the experimental pressures, are also listed in table III. Since the wall temperature is well above the boiling points of the cryogenic propellants liquid oxygen and fluorine, they could not have formed a film on the wall. Wall temperatures are well below the boiling points of heptane and hydrazine, so that they could form stable films and maintain a sizeable heat-transfer rate across the film without boiling. Since the wall temperature is near the boiling point of ammonia, this fuel could act as a film coolant. Heat transfer from the gases would cause the ammonia film to boil rather than to heat the wall. Heat transfer to the coolant would be small because the gas side of the wall is maintained at a low temperature by the boiling ammonia. The data of reference 15 indicate that 15 to 20 percent of all the ammonia injected would be needed on the wall to provide this cooling. This would not decrease η_c if the film vaporized by the time it entered the nozzle.

SUMMARY OF RESULTS

Characteristic exhaust velocity and combustion efficiency of a nominal 200-pound-thrust engine were experimentally determined for eleven propellant combinations at several chamber lengths for a spray formed by two impinging jets. Of all the propellants tested, hydrogen with any oxidant gave the highest combustion efficiency.

A comparison of the experimental results with calculations, based on the assumption that vaporization of the propellants determines the rate of combustion, showed fair agreement except for ammonia-fluorine and combinations that included hydrazine. Decomposition of the hydrazine in the liquid phase may be responsible for the anomalous behavior of hydrazine.

Over-all heat-transfer rates were also determined for each propellant combination and were compared with values calculated by standard heat-transfer equations. The calculated heat-transfer rates agree with the experimental rates for all propellant combinations except ammonia, which may have acted as a film coolant.

Lewis Research Center
National Aeronautics and Space Administration
Cleveland, Ohio, October 1, 1958

APPENDIX A

SYMBOLS

A	cross-sectional area, sq in.
c^*	characteristic exhaust velocity, ft/sec
c_x^*, c_n^*	theoretical characteristic exhaust velocity for gas phase mixture ratio occurring at point x or point n, ft/sec
D_j	injection orifice diameter, in.
D_{30}	volume-number-mean drop diameter, in.
$\mathcal{F}$	fraction of fuel vaporized, dimensionless
g	gravitational constant, ft/sec^2
L	total chamber length, in.
M	molecular weight
$M_{g,m}$	mass median drop radius produced by injector, in.
o/f	oxidant-fuel weight ratio
$\mathcal{O}$	fraction of oxidant vaporized, dimensionless
P	chamber total pressure, lb/sq in. abs
p	static pressure, lb/sq in. abs
R	molar gas constant, in./$^{\circ}$R
T	temperature, $^{\circ}$R
T^*	reduced temperature of propellant
u	gas velocity at any point, ft/sec
u_{fin}	final gas velocity reached with complete combustion before nozzle, in./sec
V_j	jet velocity, ft/sec

ΔV velocity difference between injected liquid and gases surrounding liquid jet, ft/sec

v_0 injection velocity, in./sec

W mass-flow rate in gas phase, lb/sec

w_f fuel weight flow, lb/sec

w_o oxidant weight flow, lb/sec

γ specific heat ratio, dimensionless

η_c combustion efficiency, percent of theoretical characteristic exhaust velocity or gas velocity

μ_l absolute liquid viscosity of propellant, lb/(in.)(sec)

ρ density, lb/cu in.

σ liquid surface tension of propellant, lb/in.

Subscripts:

g gaseous

l liquid

n nozzle throat

th theoretical for complete combustion

s gas stream

x point x

1 case, or point, 1

2 case, or point, 2

APPENDIX B

RELATION BETWEEN GAS VELOCITY AND PERCENT OF PROPELLANTS VAPORIZED

Gas velocity measurements are converted to percent of propellant vaporized by assuming that propellant vaporization limits the rate of combustion. The following schematic diagram is used for illustration:

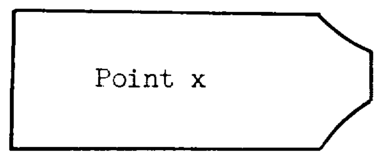

From the continuity equation,

$$u_x = \frac{W_x}{\rho_x A_x}$$

or

$$\frac{u_x}{u_{th}} = \frac{W_x \rho_{th}}{W_{th} \rho_x} \qquad \text{(B1)}$$

If the gases are assumed to follow the ideal gas law,

$$\rho_x = \frac{p_x}{R\,\frac{T_x}{M_x}}$$

or

$$\frac{\rho_{th}}{\rho_x} = \frac{p_{th}}{p_x}\,\frac{T_x/M_x}{T_{th}/M_{th}} \qquad \text{(B2)}$$

When the experimental c^* equation is used, and the static- and total-pressure ratios are assumed to be approximately equal in the chamber,

$$P_x = \frac{c_n^* W_n}{A_n g}$$

and

$$\frac{p_{th}}{p_x} = \frac{P_{th}}{P_x} = \frac{c^*_{th}W_{th}}{c^*_n W_n} \tag{B3}$$

From the theoretical c^* equation,

$$c^*_x = \frac{\sqrt{g\gamma R}}{\gamma\left(\frac{2}{\gamma + 1}\right)^{\frac{\gamma+1}{2(\gamma-1)}}}\sqrt{\frac{T_x}{M_x}}$$

Hence, if γ is assumed constant,

$$\frac{T_x/M_x}{T_{th}/M_{th}} = \frac{c^{*2}_x}{c^{*2}_{th}} \tag{B4}$$

Since

$$\left.\begin{aligned} W_x &= \mathcal{O}_x w_o + \mathcal{F}_x w_f \\ W_n &= \mathcal{O}_n w_o + \mathcal{F}_n w_f \end{aligned}\right\} \tag{B5}$$

and, combining equations ((B1) to (B5)),

$$\frac{u_x}{u_{th}} = \left(\frac{\mathcal{O}_x w_o + \mathcal{F}_x w_f}{\mathcal{O}_n w_o + \mathcal{F}_n w_f}\right)\frac{c^{*2}_x}{c^*_n c^*_{th}} \tag{B6}$$

Thus, the gas velocity efficiency at any point x is a function of the percent of fuel and oxidant vaporized at point x ($\mathcal{O}_x$ and $\mathcal{F}_x$) and at the nozzle ($\mathcal{O}_n$ and $\mathcal{F}_n$) and of the theoretical c^* values, c^*_n, c^*_x, and c^*_{th}.

For the results reported herein, the percent vaporized at the nozzle was determined from c^* measurements. The oxidant was assumed to be completely vaporized at all points in the chamber in the cases of the three propellant combinations for which gas velocity measurements were made. For the heptane - liquid-oxygen combination, the equation resulting from this assumption is plotted in figure 8.

APPENDIX C

FINAL GAS VELOCITY CALCULATIONS

In the analysis of reference 2, the final gas velocity when all of the propellants are burned is used to describe the gas velocity environment of the drop throughout its history. This final gas velocity becomes one of the correlating factors used to obtain an effective length and can be computed from the throat velocity, or from theoretical c^*, when isentropic expansion and no combustion in the nozzle are assumed.

If propellant vaporization is assumed to limit the combustion in an actual engine, the final gas velocities can be related to the actual engine efficiency as follows:

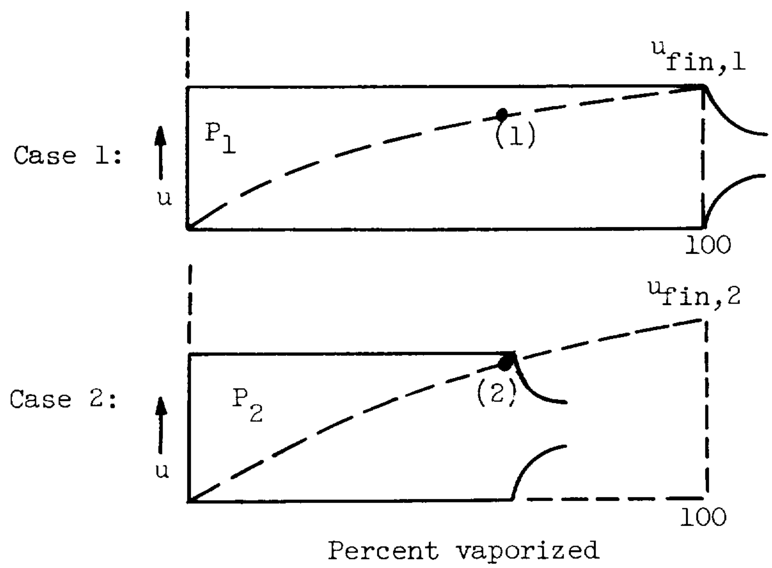

Case 1 in the diagram illustrates an engine vaporizing all the propellants. The engine of case 2 has the same propellant weight flow and chamber geometry as case 1 except that it is shorter and vaporizes only part of the propellants. The resultant inefficiency of the case 2 engine gives it a lower chamber pressure (P_2):

$$\frac{P_2}{P_1} = \frac{c_2^*}{c_1^*} = \eta_c$$

A typical gas velocity profile is shown for case 1. Point (1) in case 1 has the same percentage of the propellants vaporized as point (2) in case 2. If the T/M value of the gases is assumed to be the same at points 1 and 2, their densities will be functions only of P_1 and P_2:

$$\frac{\rho_1}{\rho_2} = \frac{P_1}{P_2} = \frac{1}{\eta_c}$$

From the continuity equation, E-112

$$\frac{u_2}{u_1} = \frac{\rho_1}{\rho_2} = \frac{1}{\eta_c}$$

To describe the gas velocity profile in case 2, a fictitious final gas velocity $(u_{fin,2})$ must be used, so that

$$\frac{u_{fin,2}}{u_{fin,1}} = \frac{u_2}{u_1} = \frac{1}{\eta_c}$$

The final gas velocities used as factors in the effective length in this correlation were obtained by dividing the theoretical gas velocity for complete combustion by the experimental engine efficiency.

APPENDIX D

HEAT-TRANSFER CALCULATIONS

Analytical heat-transfer rates were calculated for the particular engine used in this work. These calculations were made with the assumption of 100 percent combustion efficiency and a constant gas velocity along the entire chamber length. The gas-film heat-transfer coefficients were evaluated by using the Colburn equation and the averaged properties of the gases at the film temperatures.

In the experiments, 100 percent combustion efficiency was never attained. The calculated heat-transfer rates were accordingly modified for the lower chamber pressures and gas velocities at the nozzle inlet by assuming that each factor was approximately proportional to combustion efficiency. The measurements of gas velocities showed that the average gas velocity along the chamber length was about 70 percent of the velocity at the nozzle inlet. Because most of the resistance to heat transfer occurs in the gas-side film, as a close approximation the calculated over-all heat-transfer rates were multiplied by $0.7\,\eta_c^2$ to correct for the actual engine conditions.

REFERENCES

1. Heidmann, M. F., and Auble, C. M.: Injection Principles from Combustion Studies in a 200-Pound-Thrust Rocket Engine Using Liquid Oxygen and Heptane. NACA RM E55C22, 1955.

2. Priem, Richard J.: Propellant Vaporization as a Criterion for Rocket-Engine Design; Numerical Calculations of Chamber Length to Vaporize a Single n-Heptane Drop. NACA TN 3985, 1957.

3. Priem, Richard J.: Propellant Vaporization as a Criterion for Rocket-Engine Design; Calculations Using Various Log-Probability Distributions of Heptane Drops. NACA TN 4098, 1957.

4. Heidmann, Marcus F., and Priem, Richard J.: Propellant Vaporization as a Criterion for Rocket Engine Design; Relation Between Percentage of Propellant Vaporized and Engine Performance. NACA TN 4219, 1958.

5. Priem, Richard J.: Propellant Vaporization as a Criterion for Rocket-Engine Design; Calculations of Chamber Length to Vaporize Various Propellants. NACA TN 3883, 1958.

6. Gordon, Sanford, and Huff, Vearl N.: Theoretical Performance of Liquid Ammonia and Liquid Fluorine as a Rocket Propellant. NACA RM E53A26, 1953.

7. Gordon, Sanford, and Huff, Vearl N.: Theoretical Performance of Liquid Hydrazine and Liquid Fluorine as a Rocket Propellant. NACA RM E53E12, 1953.

8. Gordon, Sanford, and Huff, Vearl N.: Theoretical Performance of Liquid Hydrogen and Liquid Fluorine as a Rocket Propellant. NACA RM E52L11, 1953.

9. Huff, Vearl N., Fortini, Anthony, and Gordon, Sanford: Theoretical Performance of JP-4 Fuel and Liquid Oxygen as a Rocket Propellant. II - Equilibrium Composition. NACA RM E56D23, 1956.

10. Gordon, Sanford, and Glueck, Alan R.: Theoretical Performance of Liquid Ammonia with Liquid Oxygen as a Rocket Propellant. NACA RM E58A21, 1958.

11. Heidmann, M. F., and Auble, C. M.: Rocket Performance Measurements with Streak Photographs. Preprint No. 239-55, Am. Rocket Soc., 1955.

12. Ingebo, Robert D.: Drop-Size Distributions for Impinging-Jet Breakup in Airstreams Simulating the Velocity Conditions in Rocket Combustors. NACA TN 4222, 1958.

13. Ingebo, Robert D., and Foster, Hampton H.: Drop-Size Distribution for Crosscurrent Breakup of Liquid Jets in Airstreams. NACA TN 4087, 1957.

14. Clark, Charles C.: Hydrazine. Mathieson Chem. Corp., Baltimore (Md.), 1953.

15. Morrell, Gerald: Investigation of Internal Film Cooling of 1000-Pound-Thrust Liquid-Ammonia - Liquid-Oxygen Rocket-Engine Combustion Chamber. NACA RM E51E04, 1951.

TABLE I. - TEST CONDITIONS

Oxidant	Oxidant injection temperature, °F	Fuel	Fuel injection temperature, °F	Flow rates					o/f, Maximum theoretical c*	P, Maximum theoretical c*	c*, Maximum theoretical, equil.
				Oxidant		Fuel		Total			
				lb/sec	ft/sec	lb/sec	ft/sec				
Oxygen (l)	-320	Methane (g)	40 to 50	0.486	75.0	0.214	12.8	0.700	[a]2.27	[a]261	[a]5890
↓	↓	Heptane (l)	50 to 70	.652	65.0	.277	75.0	.929	2.35	350	5950
↓	↓	Ammonia (l)	25 to 40	.319	54.0	.251	75.0	.570	1.27	209	5800
↓	↓	Hydrazine (l)	40 to 50	.293	50.0	.406	75.0	.699	0.72	273	6174
↓	↓	Hydrogen (g)	60 to 70	.486	75.0	.152	60.5	.683	3.20	324	8010
Oxygen (g)	70 to 80	Heptane (l)	68	.652	15.1	.277	75.0	.929	2.35	353	6010
↓	45 to 75	Ammonia (l)	65 to 80	.319	12.3	.251	75.0	.570	1.27	212	5830
↓	75	Hydrazine (l)	75 to 80	.293	8.6	.406	75.0	.699	.72	276	6240
Fluorine (l)	-320	Hydrazine (l)	50	.792	60.5	.406	75.0	1.198	1.95	538	7125
↓	↓	Ammonia (l)	50	.752	57.0	.251	75.0	1.003	3.00	446	7050
↓	↓	Hydrogen (g)	50	.632	75.0	.126	40.6	.758	5.00	402	8400

[a]The liquid oxygen-gaseous methane combination was run at this o/f rather than at the o/f for maximum c*, which is 6120 feet per second, corresponding to an o/f of 2.87.

TABLE II. - EXPERIMENTAL ENGINE DATA

(a) Gaseous methane with liquid oxygen

Run	Chamber pressure, lb/sq in. abs	Oxidant flow, lb/sec	Fuel flow, lb/sec	Total flow, lb/sec	Mixture ratio, oxidant/fuel	Characteristic velocity: Experimental, ft/sec	Characteristic velocity: Percent of theoretical	Characteristic velocity: Average	Coolant flow, lb/sec	Coolant temperature rise, °F	Heat-transfer rate: Experimental, Btu/(sq in.)(sec)	Heat-transfer rate: Average, Btu/(sq in.)(sec)
Chamber length, 1 in.												
275	160	0.486	0.222	0.708	2.19	3640	61.8	59.2	----	----	-----	-----
276	163	.517	.224	.741	2.31	3470	58.4		----	----	-----	-----
277	163	.524	.224	.748	2.34	3440	57.8		----	----	-----	-----
Chamber length, 3 in.												
267	200	0.494	0.234	0.728	2.11	4320	73.5	72.6	----	----	-----	-----
269	190	.466	.228	.694	2.04	4330	74.2		----	----	-----	-----
271	185	.474	.194	.668	2.44	4370	72.8		----	----	-----	-----
272	185	.476	.197	.673	2.41	4340	72.5		----	----	-----	-----
273	183	.491	.195	.686	2.52	4210	70.0		----	----	-----	-----
Chamber length, 8 in.												
278	220	0.463	0.230	0.693	2.01	5020	86.1	84.3	3.76	8.0	0.602	0.549
279	220	.472	.225	.697	2.10	4980	85.2		1.61	16.0	.516	
280	220	.482	.215	.697	2.24	4980	84.3		1.60	15.0	.408	
281	220	.482	.220	.702	2.19	4950	84.1		1.59	16.0	.509	
282	220	.486	.220	.706	2.21	4920	83.3		----	----	-----	
283	218	.474	.225	.699	2.11	4920	83.9		3.98	6.5	.517	
284	220	.488	.220	.708	2.22	4910	83.3		4.07	7.0	.569	

(b) Heptane with liquid oxygen

Run	Chamber pressure, lb/sq in. abs	Oxidant flow, lb/sec	Fuel flow, lb/sec	Total flow, lb/sec	Mixture ratio, oxidant/fuel	Characteristic velocity: Experimental, ft/sec	Characteristic velocity: Percent of theoretical	Characteristic velocity: Average	Coolant flow, lb/sec	Coolant temperature rise, °F	Heat-transfer rate: Experimental, Btu/(sq in.)(sec)	Heat-transfer rate: Average, Btu/(sq in.)(sec)
Chamber length, 1 in.												
505	161	0.665	0.289	0.954	2.30	2660	44.7	43.9	----	----	-----	-----
506	157	.650	.285	.935	2.28	2660	44.7		----	----	-----	-----
507	160	.660	.285	.945	2.32	2680	45.1		----	----	-----	-----
508	158	.670	.289	.959	2.32	2600	43.7		----	----	-----	-----
509	156	.650	.284	.934	2.29	2640	44.4		----	----	-----	-----
510	156	.660	.286	.946	2.31	2600	43.7		----	----	-----	-----
511	155	.655	.284	.939	2.31	2610	43.8		----	----	-----	-----
512	155	.653	.281	.934	2.32	2620	44.1		----	----	-----	-----
513	159	.653	.281	.934	2.32	2690	45.3		----	----	-----	-----
514	157	.656	.284	.940	2.31	2640	44.4		----	----	-----	-----
515	153	.678	.285	.963	2.38	2510	42.2		----	----	-----	-----
516	155	.668	.301	.969	2.22	2530	42.6		----	----	-----	-----
517	156	.665	.300	.965	2.22	2560	43.1		----	----	-----	-----
Chamber length, 3 in.												
417	230	0.660	0.282	0.942	2.34	3850	64.7	65.7	----	----	-----	-----
418	232	.658	.285	.943	2.35	3890	65.4		----	----	-----	-----
419	229	.656	.277	.933	2.37	3880	65.2		----	----	-----	-----
420	231	.650	.282	.932	2.30	3910	65.7		----	----	-----	-----
421	233	.640	.281	.921	2.28	3990	67.0		----	----	-----	-----
422	232	.650	.286	.936	2.27	3910	65.7		----	----	-----	-----
423	232	.653	.282	.935	2.32	3920	65.9		----	----	-----	-----
Chamber length, 8 in.												
424	277	0.656	0.290	0.946	2.26	4620	77.8	76.2	----	----	-----	-----
425	260	.570	.315	.885	1.81	4640	78.0		----	----	-----	-----
426	270	.633	.295	.928	2.15	4590	77.3		----	----	-----	-----
427	267	.667	.286	.953	2.33	4430	74.5		----	----	-----	-----
428	267	.665	.274	.939	2.42	4490	75.4		----	----	-----	-----
431	270	.663	.269	.932	2.46	4580	77.2		3.80	14.0	1.06	1.18
432	267	.678	.270	.948	2.51	4500	75.6		3.79	14.1	1.17	
502	270	.675	.281	.956	2.40	4460	75.0		3.05	18.9	1.15	
503	270	.672	.282	.954	2.48	4470	75.2		3.14	19.4	1.22	
504	270	.667	.273	.940	2.45	4530	76.3		3.14	20.6	1.29	

TABLE II. - Continued. EXPERIMENTAL ENGINE DATA

(c) Liquid ammonia with liquid oxygen

Run	Chamber pressure, lb/sq in. abs	Oxidant flow, lb/sec	Fuel flow, lb/sec	Total flow, lb/sec	Mixture ratio, oxidant/fuel	Characteristic velocity: Experimental, ft/sec	Characteristic velocity: Percent of theoretical	Characteristic velocity: Average	Coolant flow, lb/sec	Coolant temperature rise, °F	Heat-transfer rate: Experimental, Btu/(sq in.)(sec)	Heat-transfer rate: Average, Btu/(sq in.)(sec)
						Chamber length, 1 in.						
449	108	0.342	0.260	0.602	1.31	2840	49.5	52.5	----	----	-----	-----
450	107	.324	.246	.570	1.31	2970	51.3		----	----	-----	-----
451	106	.299	.249	.548	1.20	3040	52.5		----	----	-----	-----
452	115	.299	.264	.563	1.13	3220	55.5		----	----	-----	-----
454	113	.296	.261	.557	1.13	3200	55.2		----	----	-----	-----
455	117	.326	.260	.586	1.25	3150	54.3		----	----	-----	-----
456	113	.342	.257	.599	1.13	2980	51.4		----	----	-----	-----
458	110	.314	.273	.587	1.15	2960	51.0		----	----	-----	-----
459	110	.306	.270	.576	1.13	3020	52.0		----	----	-----	-----
						Chamber length, 3 in.						
443	144	0.299	0.252	0.551	1.19	4130	71.3	70.4	----	----	-----	-----
444	146	.324	.250	.574	1.29	4020	69.4		----	----	-----	-----
445	150	.347	.253	.600	1.37	3960	68.3		----	----	-----	-----
446	147	.304	.250	.554	1.22	4190	72.3		----	----	-----	-----
447	151	.324	.248	.572	1.31	4170	72.0		----	----	-----	-----
448	154	.331	.241	.572	1.37	4260	73.5		----	----	-----	-----
469	145	.294	.257	.551	1.14	4160	71.8		----	----	-----	-----
470	147	.324	.248	.572	1.31	4060	70.1		----	----	-----	-----
471	150	.318	.249	.567	1.28	4170	71.9		----	----	-----	-----
472	148	.332	.252	.584	1.32	3970	68.5		----	----	-----	-----
473	147	.326	.250	.576	1.30	4030	69.6		----	----	-----	-----
474	151	.332	.248	.580	1.34	4100	70.7		----	----	-----	-----
476	152	.328	.253	.581	1.29	4130	71.3		----	----	-----	-----
477	150	.334	.254	.588	1.31	4030	69.7		----	----	-----	-----
478	147	.334	.253	.585	1.31	3970	68.5		----	----	-----	-----
						Chamber length, 8 in.						
434	170	0.369	0.250	0.619	1.48	4330	74.7	77.0	----	----	-----	0.243
435	165	.354	.251	.605	1.41	4300	74.1		3.40	4.0	0.272	
436	163	.321	.239	.560	1.34	4600	79.3		----	----	-----	
437	162	.327	.247	.574	1.32	4460	76.7		2.11	7.3	.309	
438	161	.321	.247	.568	1.30	4470	77.1		1.24	11.5	.286	
439	164	.334	.247	.581	1.35	4460	76.9		1.24	10.7	.276	
440	165	.331	.246	.577	1.35	4510	77.6		1.25	10.5	.263	
441	164	.334	.251	.585	1.33	4430	76.4		1.24	11.2	.278	
461	160	.318	.261	.579	1.22	4360	75.1		1.08	9.0	.194	
462	161	.302	.259	.561	1.17	4530	78.3		1.08	8.8	.190	
463	159	.306	.261	.567	1.17	4420	76.2		1.09	9.5	.207	
465	165	.308	.254	.562	1.21	4630	79.9		.855	12.1	.208	
466	161	.299	.256	.555	1.17	4580	79.0		.855	11.6	.198	
468	167	.340	.251	.591	1.36	4460	77.0		.872	13.5	.235	

(d) Hydrazine with liquid oxygen

Run	Chamber pressure, lb/sq in. abs	Oxidant flow, lb/sec	Fuel flow, lb/sec	Total flow, lb/sec	Mixture ratio, oxidant/fuel	Characteristic velocity: Experimental, ft/sec	Characteristic velocity: Percent of theoretical	Characteristic velocity: Average	Coolant flow, lb/sec	Coolant temperature rise, °F	Heat-transfer rate: Experimental, Btu/(sq in.)(sec)	Heat-transfer rate: Average, Btu/(sq in.)(sec)
						Chamber length, 1 in.						
571	178	0.246	0.397	0.643	0.620	4370	70.8	68.1	----	----	-----	-----
572	177	.240	.427	.667	.561	4190	68.0		----	----	-----	-----
573	181	.286	.404	.690	.708	4150	67.3		----	----	-----	-----
574	182	.278	.399	.677	.700	4240	68.7		----	----	-----	-----
575	188	.332	.399	.731	.831	4060	65.8		----	----	-----	-----
						Chamber length, 3 in.						
554	201	0.397	0.304	0.701	1.31	4530	73.5	74.7	----	----	-----	-----
555	207	.296	.406	.702	.976	4660	75.6		----	----	-----	-----
556	211	.309	.408	.717	.757	4650	75.4		----	----	-----	-----
557	207	.291	.422	.713	.690	4590	74.5		----	----	-----	-----
558	210	.301	.422	.723	.713	4590	74.5		----	----	-----	-----
						Chamber length, 8 in.						
563	222	0.316	0.419	0.735	0.754	4770	77.2	75.8	2.27	22.0	1.000	0.982
564	217	.308	.425	.733	.725	4680	76.0		2.28	21.5	.980	
565	217	.309	.413	.722	.748	4750	77.0		----	----	-----	
566	---	-----	-----	-----	-----	----	----		2.41	20.7	.996	
567	213	.288	.402	.690	.718	4920	79.6		2.48	20.6	1.020	
568	205	.304	.412	.716	.738	4530	73.5		2.47	19.2	.950	
569	208	.308	.408	.716	.754	4580	74.4		3.55	14.0	.996	
570	210	.328	.408	.736	.803	4510	73.1		2.46	19.0	.935	

(e) Hydrogen with liquid oxygen

Run	Chamber pressure, lb/sq in. abs	Oxidant flow, lb/sec	Fuel flow, lb/sec	Total flow, lb/sec	Mixture ratio, oxidant/fuel	Characteristic velocity: Experimental, ft/sec	Characteristic velocity: Percent of theoretical	Characteristic velocity: Average	Coolant flow, lb/sec	Coolant temperature rise, °F	Heat-transfer rate: Experimental, Btu/(sq in.)(sec)	Heat-transfer rate: Average, Btu/(sq in.)(sec)
						Chamber length, 1 in.						
519	217	0.496	0.149	0.645	3.33	5320	65.4	65.2	----	----	-----	----
520	210	.498	.157	.655	3.18	5070	63.3		----	----	-----	----
521	210	.491	.146	.637	3.36	5210	65.1		----	----	-----	----
522	215	.491	.142	.633	3.46	5370	67.1		----	----	-----	----
523	211	.493	.147	.640	3.35	5200	65.0		----	----	-----	----
						Chamber length, 3 in.						
547	253	0.501	0.152	0.653	3.30	6170	77.0	77.7	----	----	-----	----
548	254	.491	.152	.643	3.22	6250	78.0		----	----	-----	----
549	251	.488	.152	.640	3.21	6200	77.5		----	----	-----	----
550	252	.493	.152	.645	3.24	6180	77.2		----	----	-----	----
551	252	.493	.152	.645	3.24	6180	77.2		----	----	-----	----
552	255	.496	.152	.648	3.26	6220	77.6		----	----	-----	----
553	255	.488	.152	.640	3.28	6300	78.6		----	----	-----	----
						Chamber length, 8 in.						
534	290	0.481	0.141	0.629	3.40	7290	91.0	91.8	2.18	42.0	1.83	1.79
535	290	.486	.141	.627	3.44	7310	91.3		2.22	41.0	1.82	
536	290	.478	.141	.619	3.39	7400	92.4		2.22	41.6	1.84	
537	290	.496	.139	.637	3.58	7190	89.7		2.22	42.0	1.87	
539	295	.491	.142	.636	3.46	7320	91.4		2.22	39.0	1.73	
540	293	.483	.150	.633	3.22	7310	91.3		2.22	40.0	1.77	
541	295	.473	.152	.625	3.19	7460	93.1		2.21	39.5	1.75	
542	295	.478	.153	.631	3.13	7380	92.2		2.19	40.0	1.76	
544	300	.473	.157	.630	3.01	7520	93.8		2.21	39.7	1.75	
545	293	.478	.151	.629	3.17	7350	91.8		2.18	39.7	1.73	

TABLE II. - Continued. EXPERIMENTAL ENGINE DATA

(f) Heptane with gaseous oxygen

Run	Chamber pressure, lb/sq in. abs	Oxidant flow, lb/sec	Fuel flow, lb/sec	Total flow, lb/sec	Mixture ratio, oxidant/fuel	Characteristic velocity: Experimental, ft/sec	Characteristic velocity: Percent of theoretical	Characteristic velocity: Average	Coolant flow, lb/sec	Coolant temperature rise, °F	Heat-transfer rate: Experimental, Btu/(sq in.)(sec)	Heat-transfer rate: Average, Btu/(sq in.)(sec)
					Chamber length, 1 in.							
114	164	0.648	0.309	0.953	2.08	2700	44.9	44.3	----	----	-----	----
115	159	.648	.282	.930	2.30	2700	44.9		----	----	-----	----
116	160	.648	.287	.935	2.26	2700	44.9		----	----	-----	----
117	156	.648	.268	.916	2.42	2680	44.7		----	----	-----	----
118	159	.648	.280	.928	2.32	2710	45.2		----	----	-----	----
119	155	.648	.272	.920	2.38	2680	44.7		----	----	-----	----
					Chamber length, 3 in.							
107	220	0.706	0.298	1.004	2.37	3480	58.0	57.2	----	----	-----	----
108	205	.651	.294	.945	2.21	3430	57.2		----	----	-----	----
109	198	.627	.286	.913	2.19	3420	56.9		----	----	-----	----
110	198	.637	.278	.915	2.29	3420	56.9		----	----	-----	----
111	200	.658	.255	.913	2.58	3460	57.6		----	----	-----	----
112	197	.626	.281	.907	2.23	3430	57.1		----	----	-----	----
113	197	.644	.263	.907	2.45	3430	57.1		----	----	-----	----
					Chamber length, 8 in.							
120	260	0.636	0.280	0.918	2.27	4380	73.0	72.3	1.37	35.7	1.03	1.05
121	250	.636	.280	.916	2.27	4310	71.6		1.39	35.5	.987	
122	263	.665	.247	.912	2.69	4560	75.8		1.40	37.0	1.04	
123	255	.670	.266	.936	2.52	4310	71.7		1.39	38.2	1.06	
124	255	.626	.299	.925	2.09	4360	72.5		1.44	39.3	1.13	
125	253	.648	.272	.920	2.38	4350	72.4		1.42	35.8	1.02	
					(g) Ammonia with gaseous oxygen							
					Chamber length, 1 in.							
149	100	0.294	0.201	0.495	1.46	3190	54.2	55.5	----	----	-----	-----
150	105	.284	.217	.501	1.31	3310	56.2		----	----	-----	-----
151	107	.284	.240	.524	1.18	3220	54.6		----	----	-----	-----
152	107	.284	.238	.522	1.19	3240	55.0		----	----	-----	-----
153	110	.289	.240	.529	1.20	3290	55.8		----	----	-----	-----
154	110	.294	.241	.535	1.22	3250	55.2		----	----	-----	-----
155	110	.294	.237	.531	1.24	3280	55.7		----	----	-----	-----
156	110	.294	.239	.533	1.23	3260	55.3		----	----	-----	-----
157	110	.294	.240	.534	1.22	3260	55.3		---	----	-----	-----
					Chamber length, 3 in.							
132	128	0.316	0.196	0.512	1.61	3950	67.0	68.0	----	----	-----	-----
133	143	.311	.221	.532	1.41	4250	72.2		----	----	-----	-----
134	140	.320	.238	.558	1.34	3960	67.2		----	----	-----	-----
135	137	.320	.226	.546	1.42	3970	67.4		----	----	-----	-----
136	144	.302	.274	.576	1.10	3950	67.2		----	----	-----	-----
137	155	.321	.279	.600	1.15	4070	69.1		----	----	-----	-----
138	150	.321	.275	.596	1.17	3970	67.4		----	----	-----	-----
139	150	.316	.279	.595	1.12	3970	67.4		----	----	-----	-----
140	135	.334	.214	.548	1.64	3890	66.1		----	----	-----	-----
141	145	.307	.272	.579	1.13	3950	67.1		----	----	-----	-----
142	145	.302	.268	.570	1.13	4020	68.2		----	----	-----	-----
143	150	.335	.260	.595	1.29	3980	67.6		----	----	-----	-----
144	140	.331	.212	.543	1.56	4070	69.1		----	----	-----	-----
145	145	.316	.266	.582	1.19	3930	67.7		----	----	-----	-----
146	145	.328	.246	.574	1.33	3990	67.7		----	----	-----	-----
147	145	.322	.252	.574	1.28	3990	67.7		----	----	-----	-----
					Chamber length, 8 in.							
126	162	0.314	0.259	0.573	1.21	4470	75.9	74.7	1.44	8.00	0.251	0.224
127	160	.327	.243	.570	1.34	4430	75.3		1.49	8.00	.258	
128	164	.305	.278	.583	1.09	4440	75.4		1.48	7.80	.231	
129	165	.322	.266	.588	1.21	4450	75.3		1.41	8.50	.240	
130	163	.322	.260	.582	1.24	4420	75.0		1.39	8.50	.236	
131	165	.322	.259	.581	1.24	4490	76.2		1.41	8.80	.248	
217	161	.320	.283	.593	1.13	4280	72.8		1.02	9.25	.189	
218	163	.328	.268	.596	1.22	4320	73.4		1.10	10.00	.220	
219	157	.309	.273	.582	1.13	4270	72.5		1.08	9.25	.200	
220	159	.320	.260	.580	1.23	4330	73.7		1.17	9.40	.220	
221	159	.319	.265	.584	1.20	4300	73.1		1.17	9.50	.222	
222	158	.318	.261	.579	1.22	4310	73.2		1.18	9.40	.228	
223	156	.318	.244	.562	1.30	4390	74.6		1.26	9.00	.227	
					(h) Hydrazine with gaseous oxygen							
					Chamber length, 1 in.							
175	182	0.303	0.407	0.710	0.744	4050	65.0	65.	----	----	-----	-----
176	180	.277	.412	.689	.672	4120	66.1		----	----	-----	-----
177	180	.283	.407	.690	.695	4120	66.1		----	----	-----	-----
178	180	.286	.407	.693	.703	4110	66.0		----	----	-----	-----
179	180	.291	.407	.698	.714	4080	65.7		----	----	-----	-----
180	180	.294	.408	.702	.720	4050	65.0		----	----	-----	-----
181	182	.286	.408	.694	.700	4140	66.5		----	----	-----	-----
182	180	.291	.408	.699	.713	4170	67.0		----	----	-----	-----
					Chamber length, 3 in.							
171	203	0.291	0.412	0.703	0.707	4560	73.1	73.	----	----	-----	-----
172	202	.287	.407	.694	.702	4600	73.7		----	----	-----	-----
173	200	.287	.410	.697	.700	4530	72.6		----	----	-----	-----
174	202	.287	.410	.697	.700	4580	73.5		----	----	-----	-----
					Chamber length, 8 in.							
204	210	0.300	0.430	0.730	0.697	4540	72.8	74.	1.30	31.0	0.806	0.805
205	---	-----	-----	-----	-----	----	----		1.16	35.1	.815	
206	---	-----	-----	-----	-----	----	----		1.15	35.0	.805	
207	210	.300	.414	.714	.724	4640	74.3		1.16	34.0	.780	
208	213	.317	.406	.723	.780	4660	74.6		1.20	34.0	.818	
209	215	.322	.392	.714	.821	4760	76.2		1.20	33.5	.804	
210	205	.292	.416	.708	.703	4570	73.2		----	-----	-----	-----

TABLE II. - Concluded. EXPERIMENTAL ENGINE DATA

(i) Hydrazine with fluorine

Run	Chamber pressure, lb/sq in. abs	Oxidant flow, lb/sec	Fuel flow, lb/sec	Total flow, lb/sec	Mixture ratio, oxidant/fuel	Characteristic velocity: Experimental, ft/sec	Characteristic velocity: Percent of theoretical	Characteristic velocity: Average	Coolant flow, lb/sec	Coolant temperature rise, °F	Heat-transfer rate: Experimental, Btu/(sq in.)(sec)	Heat-transfer rate: Average, Btu/(sq in.)(sec)
Chamber length, 1 in.												
347	305	0.681	0.404	1.084	1.68	4430	62.5	57.6	----	----	----	----
348	298	.856	.396	1.252	2.16	3760	52.8	↓	----	----	----	----
Chamber length, 3 in.												
340	390	0.911	.391	1.302	2.33	4730	66.4	66.7	----	----	----	----
341	353	.775	.404	1.179	1.92	4730	66.4	↓	----	----	----	----
342	353	.775	.408	1.183	1.90	4710	66.0	↓	----	----	----	----
343	360	.775	.396	1.171	1.96	4850	68.0	↓	----	----	----	----
Chamber length, 8 in.												
344	410	0.760	0.412	1.172	1.85	5520	77.5	78.6	2.82	29.0	1.64	1.64
345	423	.781	.398	1.179	1.96	5680	79.7	↓	2.80	29.5	1.65	↓
346	427	.795	.402	1.197	1.98	5620	78.7	↓	2.32	24.5	1.63	↓

(j) Liquid ammonia with liquid fluorine

Run	Chamber pressure, lb/sq in. abs	Oxidant flow, lb/sec	Fuel flow, lb/sec	Total flow, lb/sec	Mixture ratio, oxidant/fuel	Characteristic velocity: Experimental, ft/sec	Characteristic velocity: Percent of theoretical	Characteristic velocity: Average	Coolant flow, lb/sec	Coolant temperature rise, °F	Heat-transfer rate: Experimental, Btu/(sq in.)(sec)	Heat-transfer rate: Average, Btu/(sq in.)(sec)
Chamber length, 1 in.												
328	170	0.575	0.279	0.854	2.06	3170	45.0	43.4	----	----	----	----
329	190	.717	.257	.974	2.79	3090	43.7	↓	----	----	----	----
330	192	.850	.258	1.108	3.29	2740	38.4	↓	----	----	----	----
Chamber length, 3 in.												
325	310	0.886	0.276	1.162	3.21	4210	59.7	58.9	----	----	----	----
326	273	.775	.258	1.033	3.00	4170	59.2	↓	----	----	----	----
327	267	.781	.257	1.038	3.04	4070	57.7	↓	----	----	----	----
Chamber length, 8 in.												
333	345	0.810	0.271	1.081	2.99	5040	71.6	71.9	4.66	13.0	1.21	1.27
334	337	.826	.259	1.085	3.32	4910	69.6	↓	4.70	14.0	1.32	↓
335	335	.801	.265	1.066	3.02	4970	70.5	↓	4.70	13.0	1.22	↓
336	315	.659	.274	.933	2.40	5340	75.9	↓	4.63	14.2	1.32	↓

(k) Hydrogen with fluorine

Run	Chamber pressure, lb/sq in. abs	Oxidant flow, lb/sec	Fuel flow, lb/sec	Total flow, lb/sec	Mixture ratio, oxidant/fuel	Characteristic velocity: Experimental, ft/sec	Characteristic velocity: Percent of theoretical	Characteristic velocity: Average	Coolant flow, lb/sec	Coolant temperature rise, °F	Heat-transfer rate: Experimental, Btu/(sq in.)(sec)	Heat-transfer rate: Average, Btu/(sq in.)(sec)
Chamber length, 1 in.												
316	283	0.646	0.143	0.789	4.52	5660	67.4	67.6	----	----	----	----
317	275	.634	.128	.762	4.96	5700	67.8	↓	----	----	----	----
318	277	.656	.136	.792	4.83	5520	65.7	↓	----	----	----	----
319	280	.624	.134	.758	4.66	5830	69.4	↓	----	----	----	----
Chamber length, 3 in.												
312	291	0.601	0.107	0.708	5.62	6500	77.4	78.6	----	----	----	----
313	330	.636	.151	.787	4.21	6610	78.6	↓	----	----	----	----
314	330	.636	.141	.777	4.51	6710	79.8	↓	----	----	----	----
315	321	.643	.129	.772	4.98	6570	79.5	↓	----	----	----	----
Chamber length, 8 in.												
320a	317	0.523	0.141	0.664	3.71	7550	89.9	89.9	----	----	----	----
320b	337	.591	.115	.706	5.37	7540	89.7	↓	----	----	----	----
321	---	-----	-----	-----	----	----	----	↓	4.48	27.5	2.46	2.49
322	315	.491	.156	.647	3.14	7580	90.1	↓	----	----	----	↓
323	---	-----	-----	-----	----	----	----	----	4.20	30.0	2.52	↓

TABLE III. - AVERAGE HEAT-TRANSFER RESULTS

Propellants		Heat-transfer rates, Btu/(sq in.)(sec)			Ratio of experimental heat transfer to analytical, actual efficiency	Calculated gas side wall temperature, °F	Boiling temperature of propellant in impinging jets, °F
Fuel	Oxidant	Analytical		Experimental			
		At 100 percent efficiency	At actual efficiency				
Heptane	Oxygen (l)	2.82	1.15	1.18	1.03	294	460
Ammonia	↓	2.07	.860	.243	.283	127	81
Hydrazine	↓	2.49	.984	.982	.996	224	430
Hydrogen	↓	3.04	1.84	1.79	.972	356	-220
Heptane	Oxygen (g)	2.80	1.04	1.05	1.01	279	460
Ammonia	↓	2.10	.815	.224	.275	120	76
Hydrazine	↓	2.50	.967	.805	.833	246	420
Ammonia	Fluorine (l)	4.48	1.62	1.27	.784	212	126
Hydrazine	↓	5.14	2.07	1.64	.792	293	500
Hydrogen	↓	4.08	2.37	2.49	1.05	356	-226

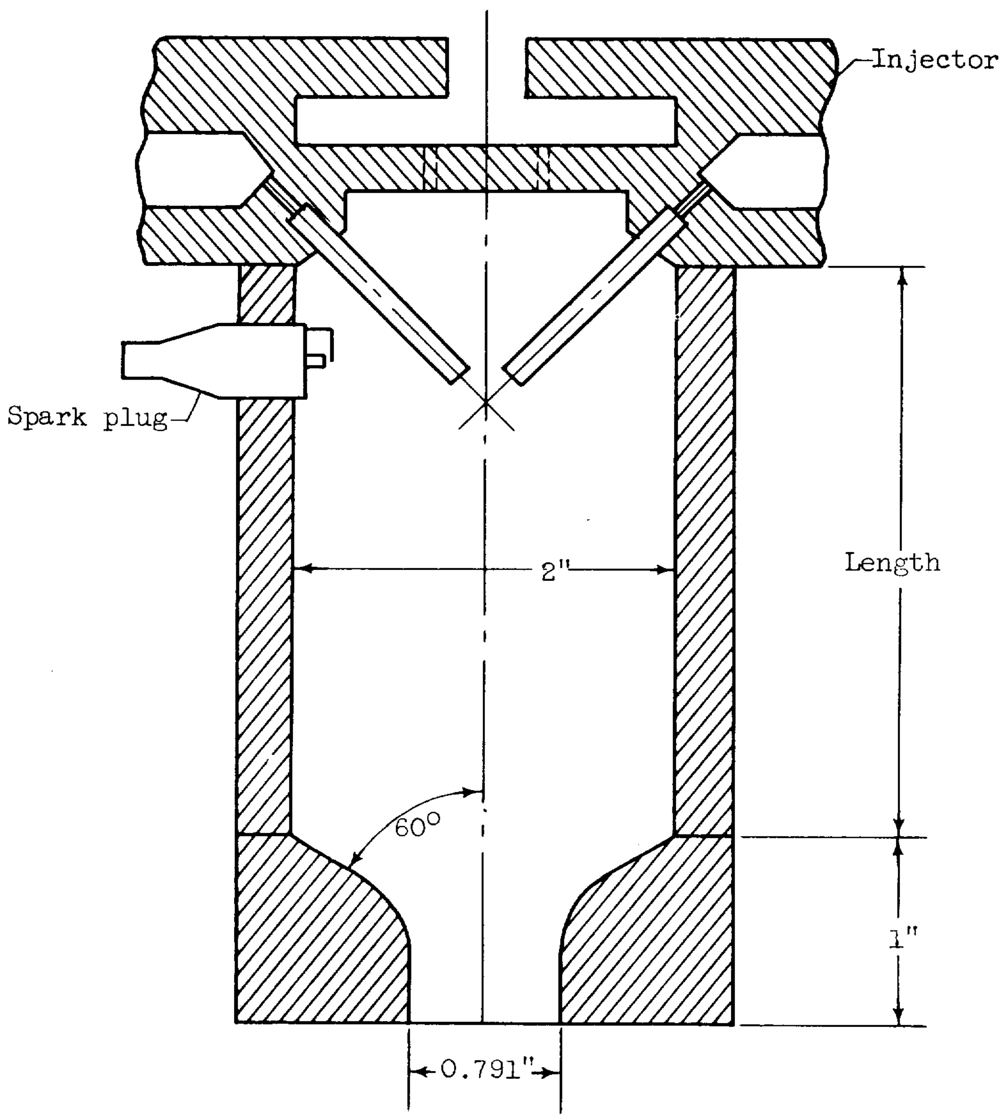

Figure 1. - Rocket engine.

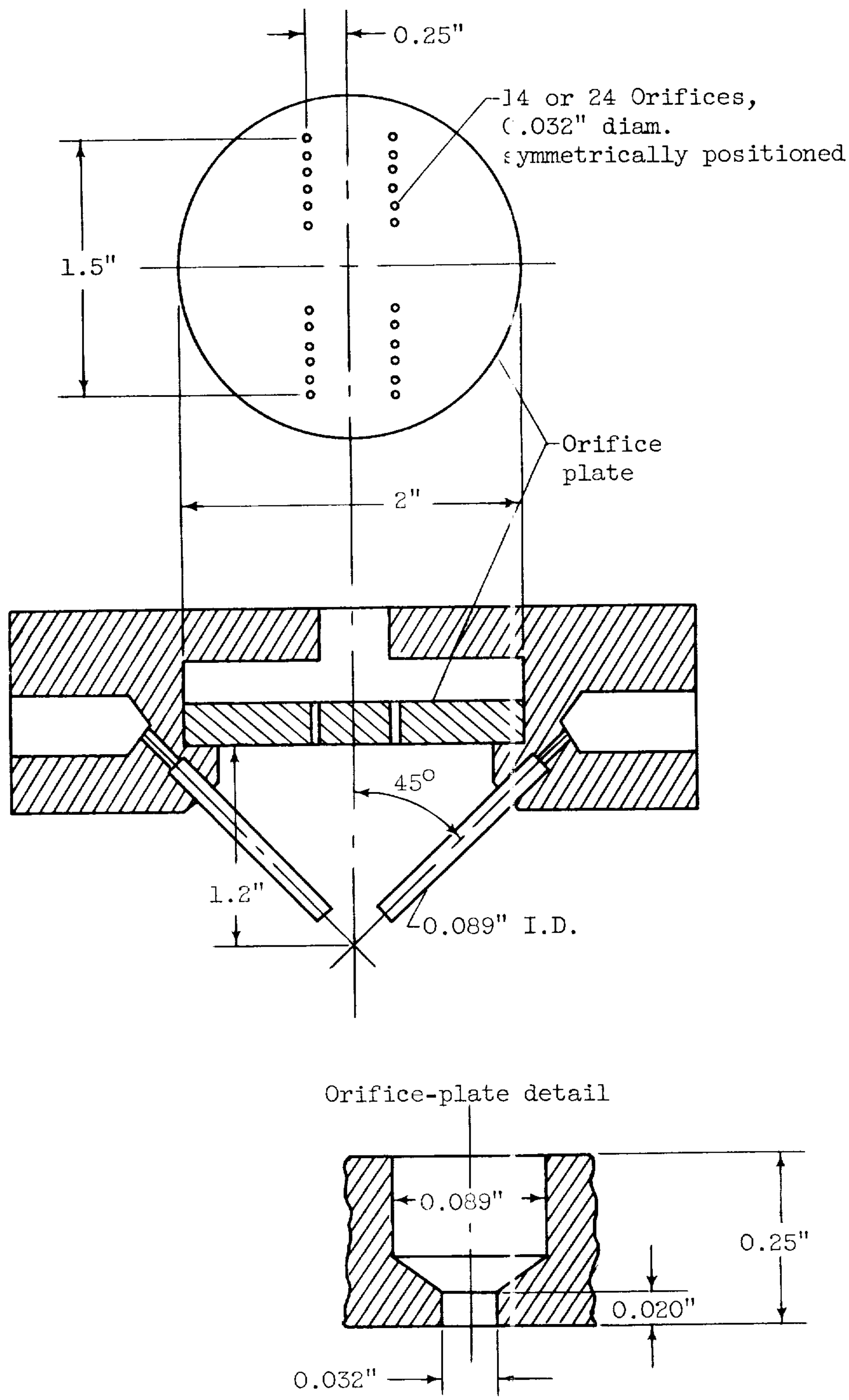

Figure 2. - Liquid-liquid injector.

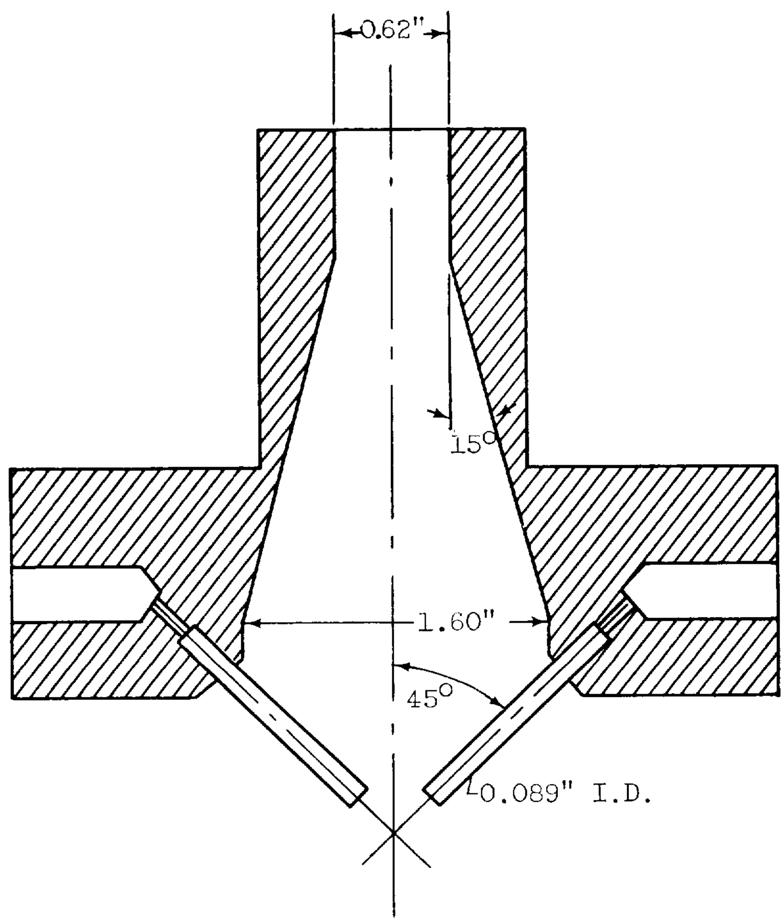

Figure 3. - Liquid-gaseous injector.

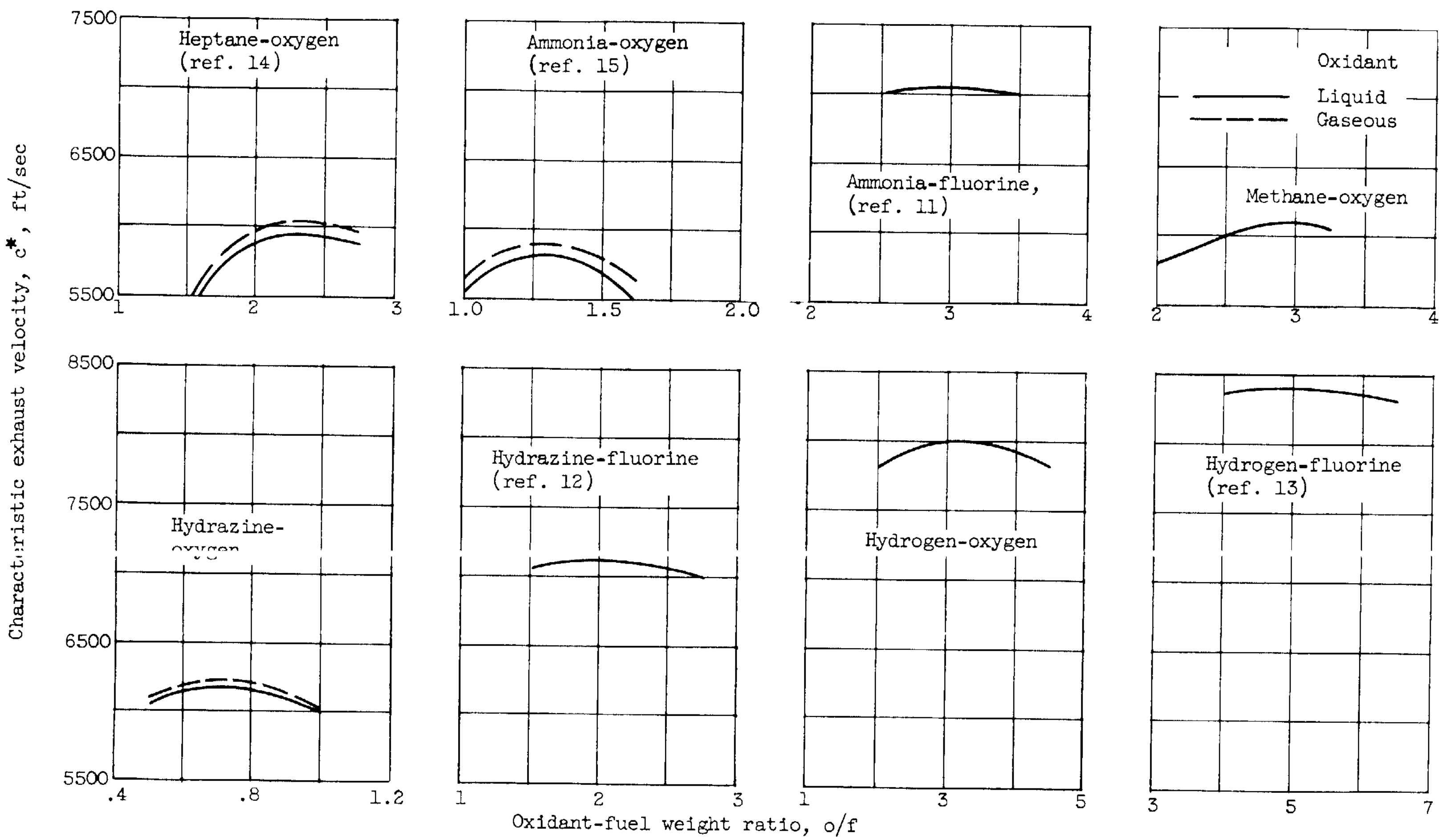

Figure 4. - Theoretical exhaust velocities as functions of oxidant-fuel weight ratios for various propellants.

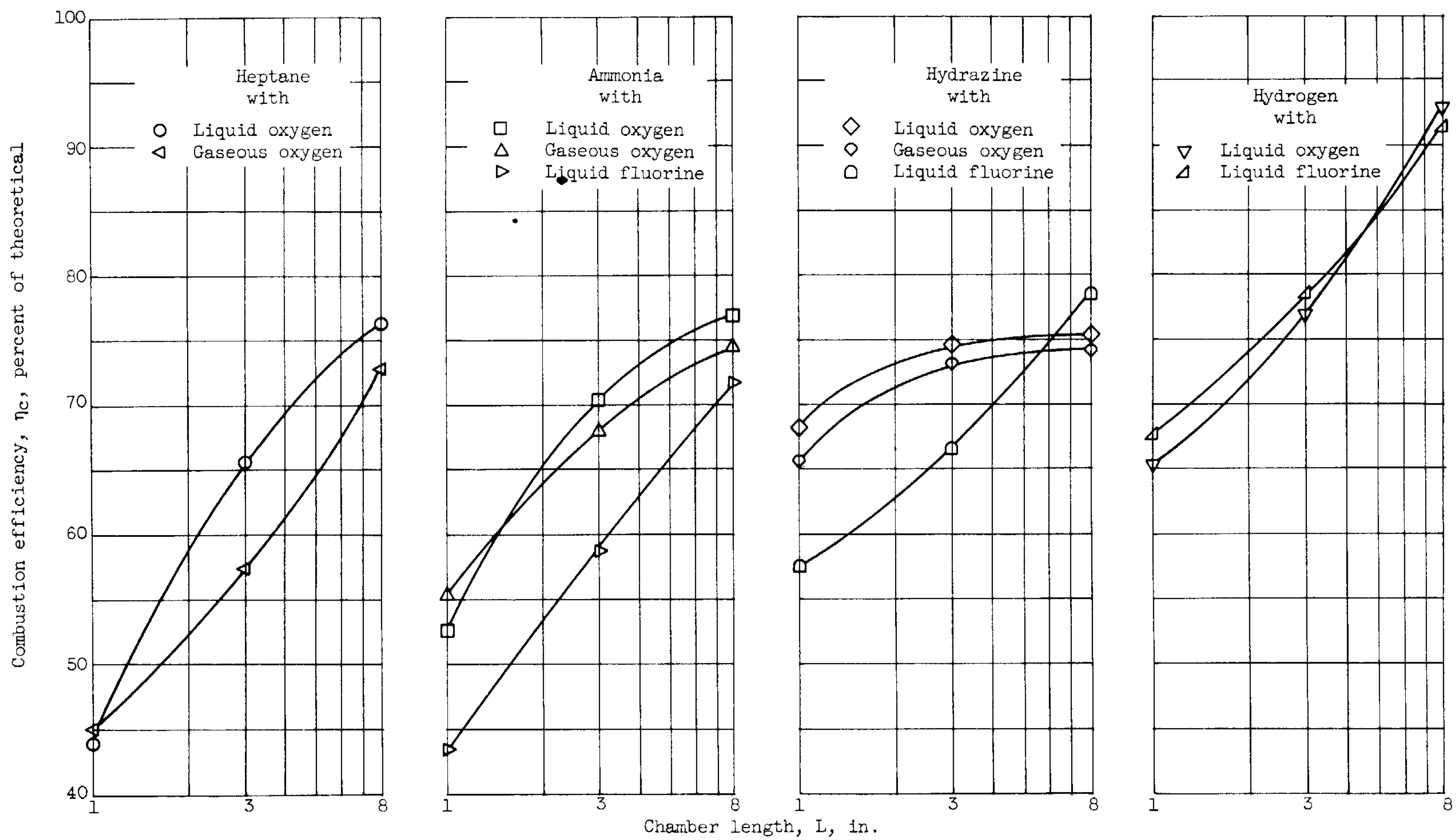

(a) Fuels with various oxidants.

Figure 5. - Performance results comparing various oxidants and fuels.

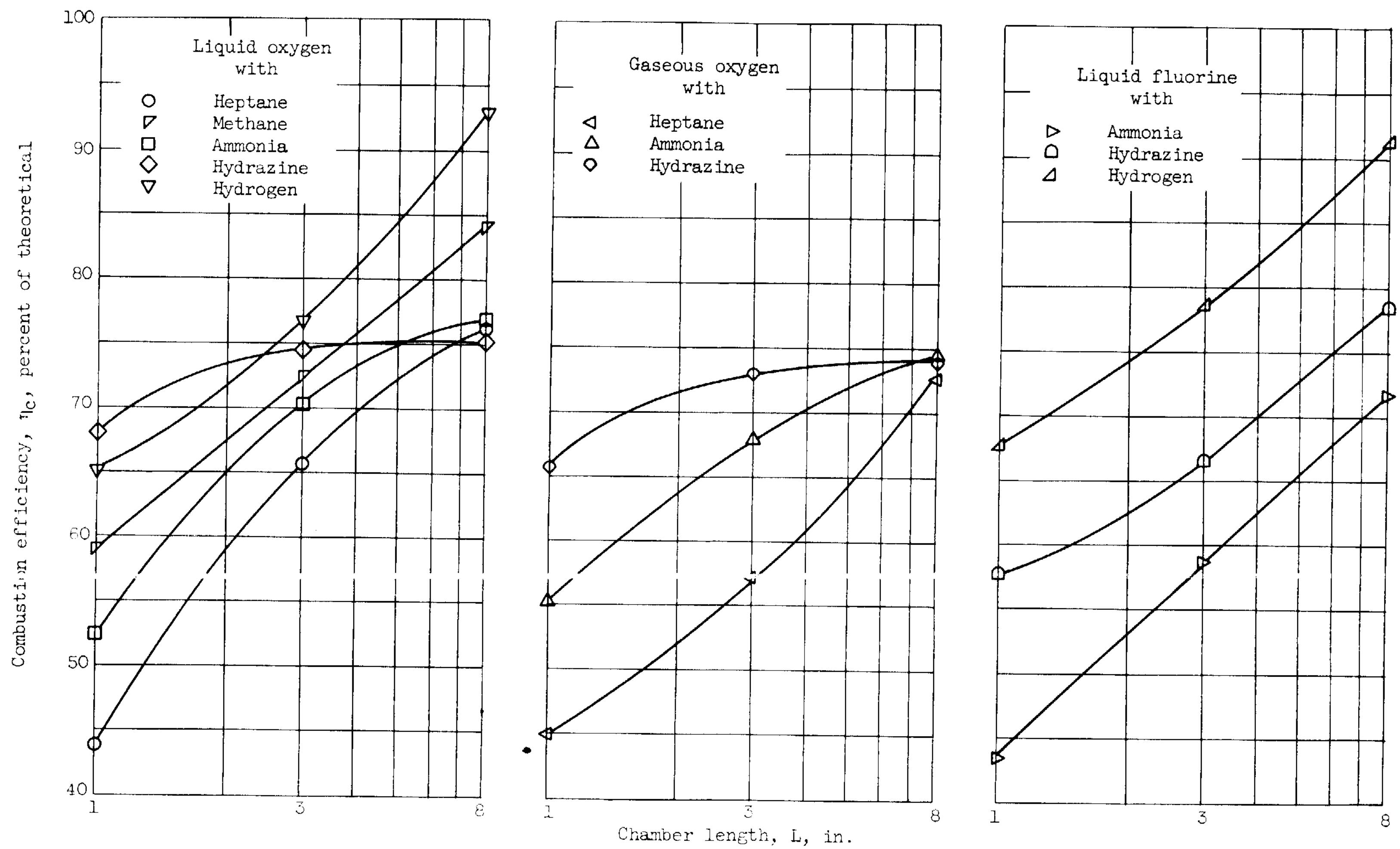

(b) Oxidants with various fuels.

Figure 5. - Concluded. Performance results comparing various oxidants and fuels.

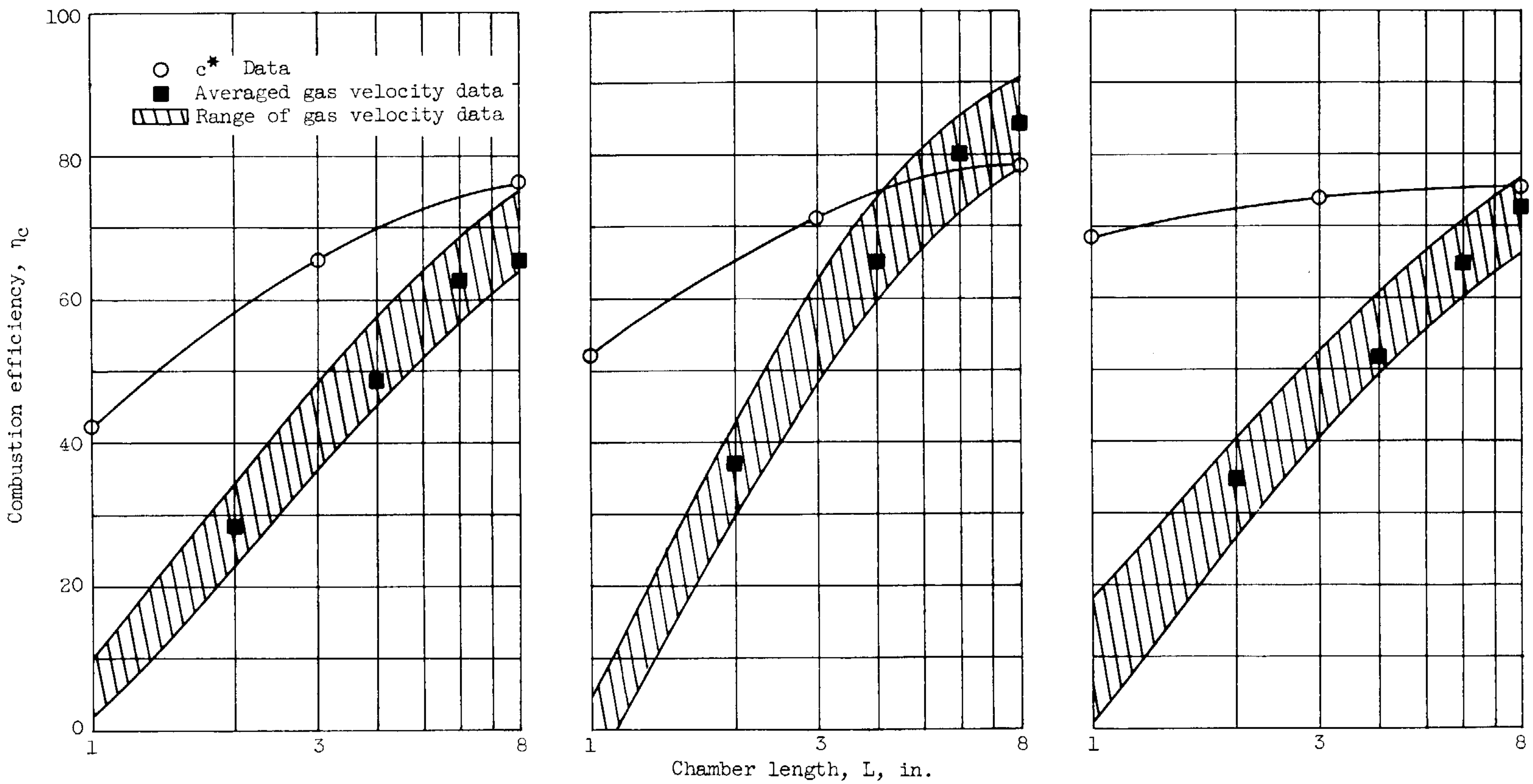

(a) Heptane with liquid oxygen.

(b) Ammonia with liquid oxygen.

(c) Hydrazine with liquid oxygen.

Figure 6. - Comparison of combustion efficiencies obtained from characteristic exhaust velocities and chamber gas velocities for various propellant combinations.

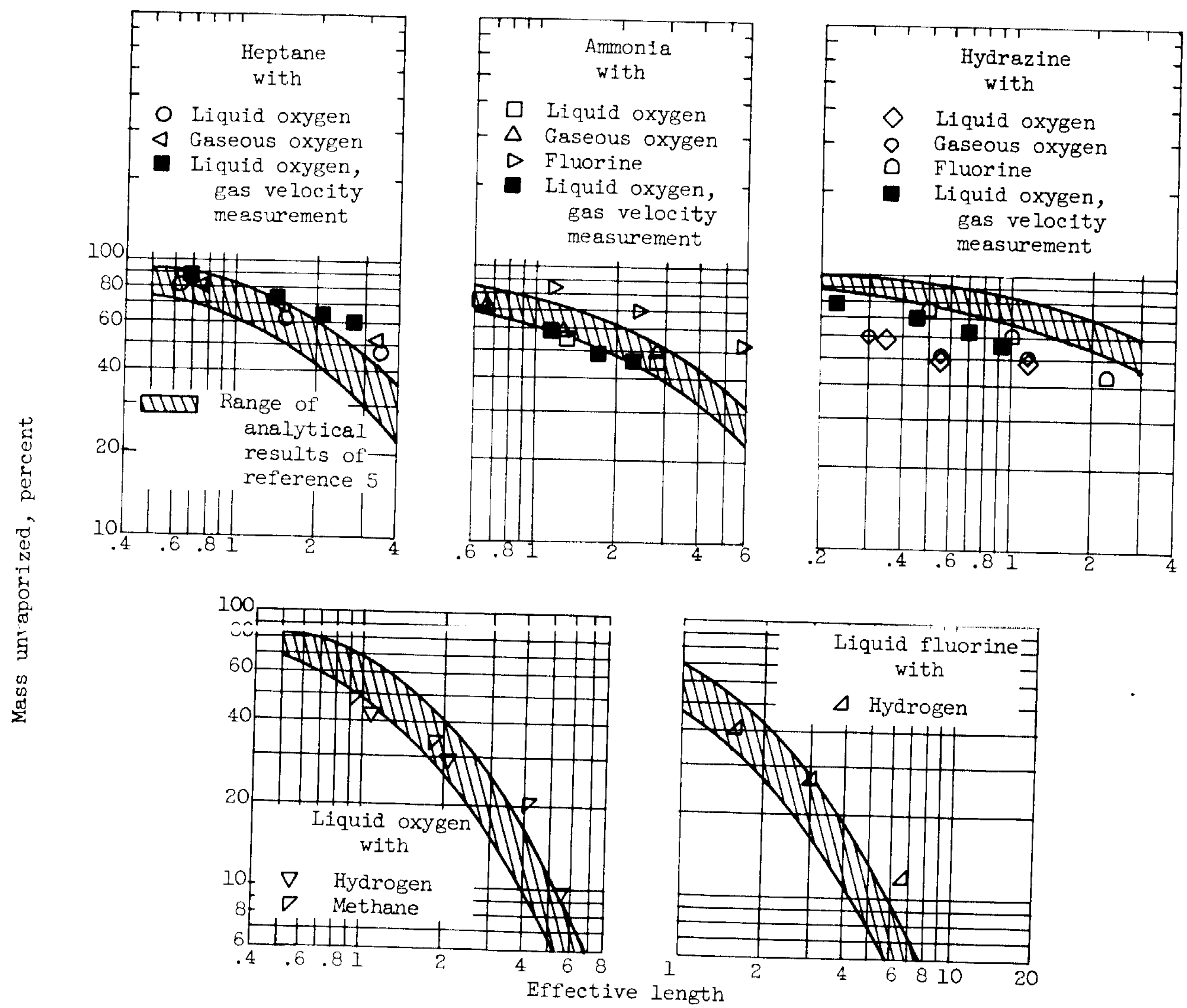

Figure 7. - Comparison of experimental and analytical results, using the model of propellant vaporization as the rate-controlling process.

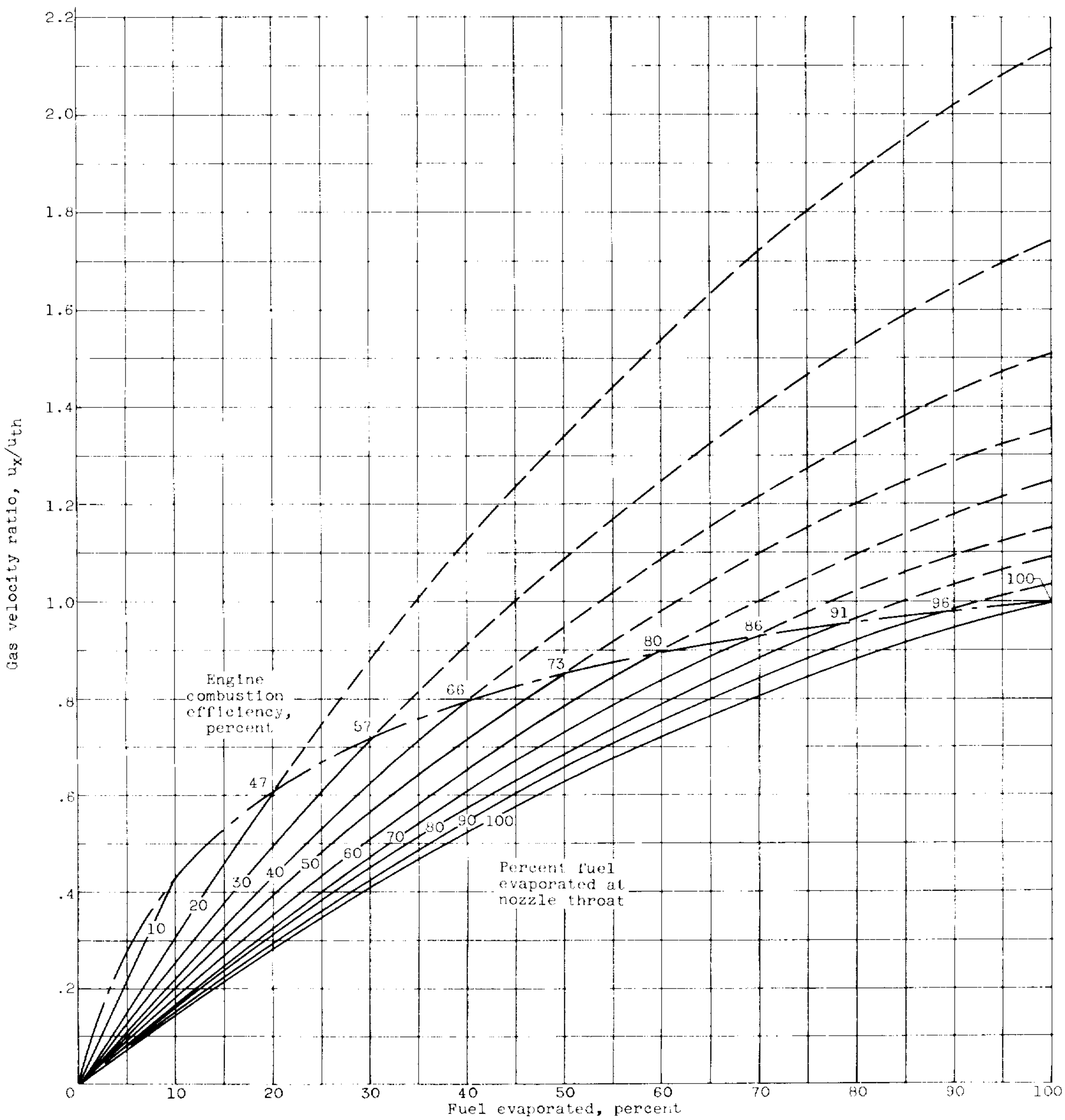

Figure 8. - Gas velocity ratios for various amounts of fuel evaporated. Heptane with liquid oxygen at an oxidant-fuel ratio of 2.5.